Real-Space Topology-Engineering of Skyrmionic Spin Textures in a van der Waals Ferromagnet Fe$_3$GaTe$_2$

Shuo Mi,[+] Jianfeng Guo,[+] Guojing Hu, Guangcheng Wang, Songyang Li, Zizhao Gong, Shuaizhao Jin, Rui Xu, Fei Pang, Wei Ji, Weiqiang Yu, Xiaolei Wang,* Xueyun Wang,* Haitao Yang,* and Zhihai Cheng*

Cite This: https://doi.org/10.1021/acs.nanolett.4c04031

Read Online

ACCESS | Metrics & More | Article Recommendations | SI Supporting Information

ABSTRACT: Realizing magnetic skyrmions in two-dimensional (2D) van der Waals (vdW) ferromagnets offers unparalleled prospects for future spintronic applications. The room-temperature ferromagnet Fe$_3$GaTe$_2$ provides an ideal platform for tailoring these magnetic solitons. Here, skyrmions of distinct topological charges are artificially introduced and engineered by using magnetic force microscopy (MFM). The skyrmion lattice is realized by a specific field-cooling process and can be further erased and painted via delicate manipulation of the tip stray field. The skyrmion lattice with opposite topological charges ($S = \pm 1$) can be tailored at the target regions to form topological skyrmion junctions (TSJs) with specific configurations. The delicate interplay of TSJs and spin-polarized device current were finally investigated via the *in situ* transport measurements, alongside the topological stability of TSJs. Our results demonstrate that Fe$_3$GaTe$_2$ not only serves as a potential building block for skyrmion-based spintronic devices, but also presents prospects for Fe$_3$GaTe$_2$-based heterostructures with the engineered topological spin textures.

KEYWORDS: skyrmion, topology-engineering, topological skyrmion junctions, magnetic force microscopy, van der Waals ferromagnets
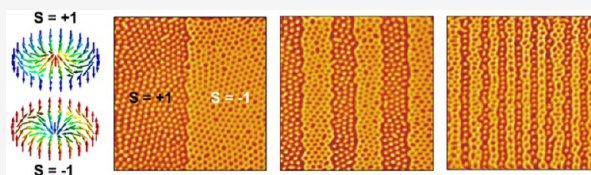
Topological magnetic textures have emerged as promising candidates for future spintronic devices, offering unique properties that could revolutionize information storage and processing.[1−3] Among these textures, magnetic skyrmions are nanoscale swirling spin textures exhibiting nontrivial real-space topology.[4] Currently, magnetic skyrmions are being considered for advanced spintronic devices, including racetrack memories, logic gates, and neuromorphic computing, and so on, due to their stability, small size, and controllable responses to external manipulations.[5] Furthermore, their low energy-cost current-driven motion favors their potential for practical applications.[6−9] These compelling features present new opportunities for exploring nontrivial topological physics and hold significant promise for future spintronics. To realize skyrmion-based spintronic devices with high integration levels and superior performance, it is crucial to achieve effective control over skyrmion properties, including their size, density, and stability.[10,11]

Magnetic skyrmions are characterized by parameters such as core polarity, vorticity, and in-plane circular magnetization. Changes in these parameters result in significant variations in skyrmion properties. For instance, skyrmions with different topological charges exhibit a contrasting topological Hall effect and skyrmion Hall effect.[12−15] Currently, the regulation of skyrmions with different topological charges can be achieved through various macroscopic methods, such as external stimuli (e.g., strain, electric fields, thermal effects, and laser

pulses).[16−18] However, the manipulation of skyrmions with different topological charges by the microscopic method has not been fully explored. If modulation of the topological order can be achieved locally, then unprecedented heterostructures of skyrmions could be realized. This unique magnetic structure may exhibit unexpected electrical properties, thereby advancing the development of spintronics.

Two-dimensional (2D) van der Waals (vdW) magnets have recently become attractive platforms for topology-based spintronics due to their fascinating physical properties, such as giant tunneling magnetoresistance and strong spin−orbit coupling. In recent years, materials, such as Cr$_2$Ge$_2$Te$_6$,[19] CrI$_3$,[20] Fe$_n$GeTe$_2$ (n = 3, 4, or 5),[21−27] and CrTe$_2$,[28] have been demonstrated to generate magnetic skyrmions. For example, the domain walls (DWs) in Fe$_3$GeTe$_2$ can be driven by current pulses, enabling controlled resistive state switching.[26,27] Similarly, different skyrmion phases provide additional degrees of freedom for the design of compact and energy-efficient spintronic devices based on topology. These complexities
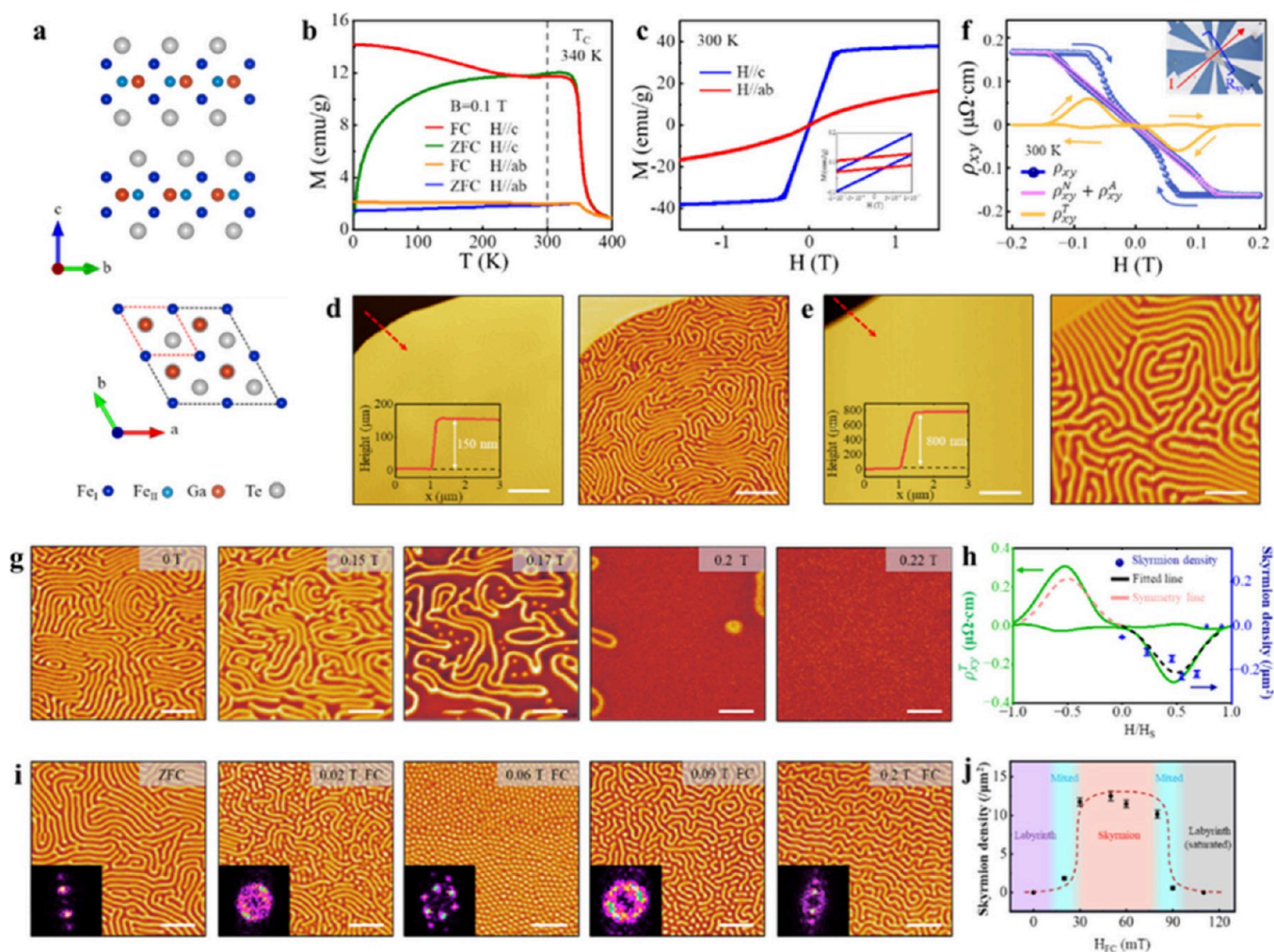
Figure 1. Structural and magnetic characterization of Fe_3GaTe_2. (a) Side- and top-view of the crystal structure. (b) Temperature dependence of zero-field-cooled (ZFC) and field-cooled (FC) magnetizations. (c) Field-dependent magnetizations ($M-H$) at 300 K under the $H // ab$ and $H // c$. (d,e) Topography images and corresponding MFM images of Fe_3GaTe_2 flakes with thicknesses of 150 nm (d) and 800 nm (e). (f) Hall resistivity ρ_{xy}, normal and anomalous Hall resistivity $\rho_{xy}^N + \rho_{xy}^A$, and topological Hall resistivity ρ_{xy}^T as functions of H for a Fe_3GaTe_2 flake (200 nm) at 300 K. (g) MFM images of Fe_3GaTe_2 flake with increasing magnetic fields at room temperature. The magnetic field is parallel to c and considered to be positive in the upward direction. (h) ρ_{xy}^T and skyrmion density derived from (g) versus H for the flake. The black dashed line represents the fit curve derived from the skyrmion density, while the pink dashed line is derived from the center inversion. (i) MFM images obtained at 0 T after different FC. The insets show the corresponding FFT maps. (j) Skyrmion density curve obtained from data fits in (i), showing different magnetic phases. Scale bar: 2 μm.

present challenges in racetrack memory devices. Additionally, recent studies demonstrated that Fe_3GaTe_2 exhibits ferromagnetism and topological Hall effects at room temperature,[29−38] suggesting its potential to host room-temperature skyrmions. The presence of Fe vacancies induces a deviation in the central positions of Fe atoms in Fe_3GaTe_2, thereby breaking the inversion symmetry and introducing Dzyaloshinskii−Moriya (DM) interactions, ultimately resulting in formation of Néel-type skyrmions.[33,39] Therefore, the discovery of the vdW ferromagnet Fe_3GaTe_2 offers a promising platform for the manipulation of skyrmions at room temperature and provides us with experimental conditions to realize topology engineering of skyrmionic spin textures.

In this work, we demonstrate successful manipulation of skyrmions in Fe_3GaTe_2 using magnetic force microscopy (MFM) under external magnetic fields, achieving unprecedented spatial resolution and control. First, by field cooling (FC), a skyrmion lattice is realized and restricted in a specific range of magnetic fields. Subsequently, controllable painting

and erasing of skyrmions is succeeded by delicate manipulation of tip stray field. In particular, by combining magnetic fields, we developed a method for painting skyrmions with different topological charges in Fe_3GaTe_2, and achieved coexisting skyrmions with opposite topological charges ($S = \pm 1$). This painting technique introduces a promising binary bit representation for skyrmion storage devices. Application of the painting technique enabled us to fabricate a unique topological skyrmion junction (TSJ). This TSJ not only enhances electron transmission rates and reduces device resistance but also serves as an excellent candidate for stacking substrates, capable of providing periodic magnetic fields and topological charges. Finally, the evolution of the TSJ properties in magnetic fields reveals that skyrmions with different topological charges exhibit diverse topological properties. Our results not only demonstrate potential applications of Fe_3GaTe_2 as a storage device, but also contribute to the understanding of topological spin textures.
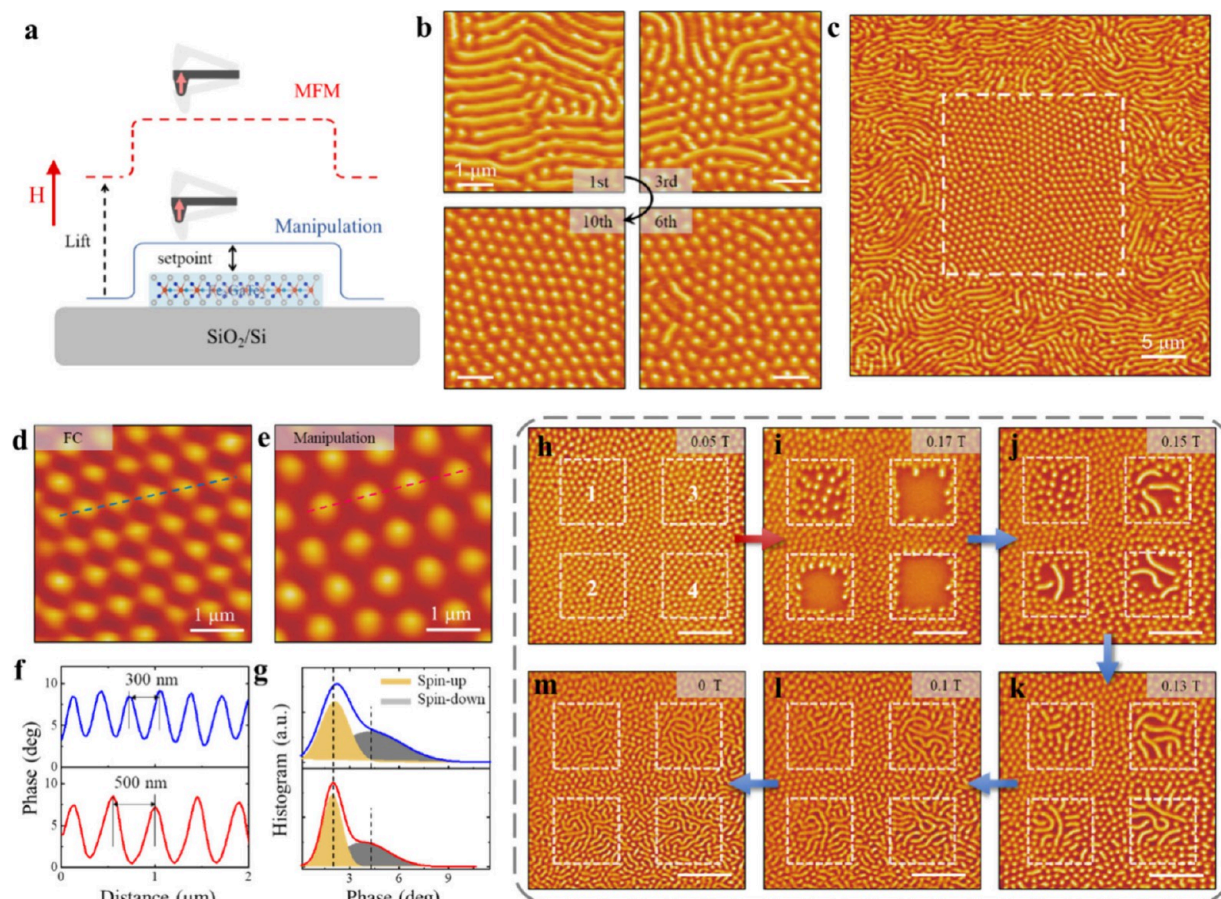
B

Figure 2. Formation and erasure manipulations of skyrmions on Fe_3GaTe_2 flake (200 nm) at 300 K. (a) Schematic diagram of manipulating skyrmions using a magnetic tip. (b) MFM images of the skyrmions generation processed at 0.05 T, corresponding to first, third, sixth and tenth manipulations, respectively. (c) Large-scale MFM image after manipulating the generation of skyrmions. The manipulation area is indicated by the white dashed box. (d,e) Skyrmions generation by FC (d) and by manipulation (e) under a constant field of 0.05 T. (f) Line profiles along the blue (d) and red (e) dashed lines. (g) Histograms of MFM signals for parts (d) and (e). (h,i) MFM images before (h) and after (i) erasing skyrmions. The white dashed line delineates the manipulation region and marks the number of manipulations. (j−m) MFM images with decreasing magnetic fields after erasing skyrmions. Scale bar: (b,d,e) 1 μm; (c,h,k) 5 μm.

Fe_3GaTe_2 is a member of the vdW ferromagnet family, in which each layer consists of a Fe_3Ga layer sandwiched by Te layers, as shown in Figure 1a. The crystal structure of Fe_3GaTe_2 corresponds to the $P6_3/mmc$ space group, which exhibits centrosymmetry with lattice parameters $a = b \approx 3.99$ Å and $c \approx 16.23$ Å.[29−31,33,34,38] The $M-T$ curves reveal that the T_C of Fe_3GaTe_2 reaches 340 K, surpassing that of most known vdW ferromagnets, as shown in Figure 1b. The variable temperature $M-H$ curves confirm the high T_C of Fe_3GaTe_2 and demonstrate that an easy magnetization axis aligns with the crystalline c-axis, as shown in Figure 1c and Figure S1. In addition, the X-ray diffraction pattern and Raman spectra demonstrate high quality of the single crystals used in our experiments (Figure S1). The Fe_3GaTe_2 flakes obtained through mechanical exfoliation were characterized by MFM at room temperature, as shown in Figure 1d,e. The real space images show that Fe_3GaTe_2 exhibits an FM labyrinthine domain in the ground state, and the domain width is clearly influenced by thickness. Specifically, the domains width increases with the thickness of Fe_3GaTe_2 flakes, following Kittel's law (Figure S2).

The EDS spectrum reveals an approximate Fe:Ga:Te ratio of 2.8:1:1.9, indicating the presence of Fe deficiency in the flakes (Figure S1). According to previous reports,[39] the presence of

Fe deficiency in Fe_3GaTe_2 introduces DM interactions, which results in the formation of topological spin textures. To verify this, we performed Hall measurements on the flake, as shown in Figure 1f, and extracted the topological Hall resistance, as in previous studies.[31] The observation of topological Hall resistivity (ρ_{xy}^T) suggests the possible existence of the topological Hall effect, which is widely regarded as a key transport signature of topological spin configurations.[32,38] Further MFM measurements confirm that the topological spin textures in Fe_3GaTe_2 correspond to magnetic skyrmions, as shown in Figure 1g. The increase in magnetic field leads to a decrease in the number of labyrinthine domains in Fe_3GaTe_2, accompanied by the generation of skyrmions. The fitting curve of skyrmion density, obtained from the MFM image, exhibits general agreement with the ρ_{xy}^T curve, thus proving the topological Hall effect as shown in Figure 1h.

To achieve a uniform skyrmion lattice, we conducted field-cooling experiments at various magnetic fields on the Fe_3GaTe_2 flake (details are provided in Figure S3) and subsequently performed MFM measurements after removing the magnetic field, as shown in Figure 1i. The characterization revealed the presence of three distinct magnetic phases, namely labyrinthine domain, mixed phase, and skyrmion lattice. Among them, the skyrmion lattice manifest within the range
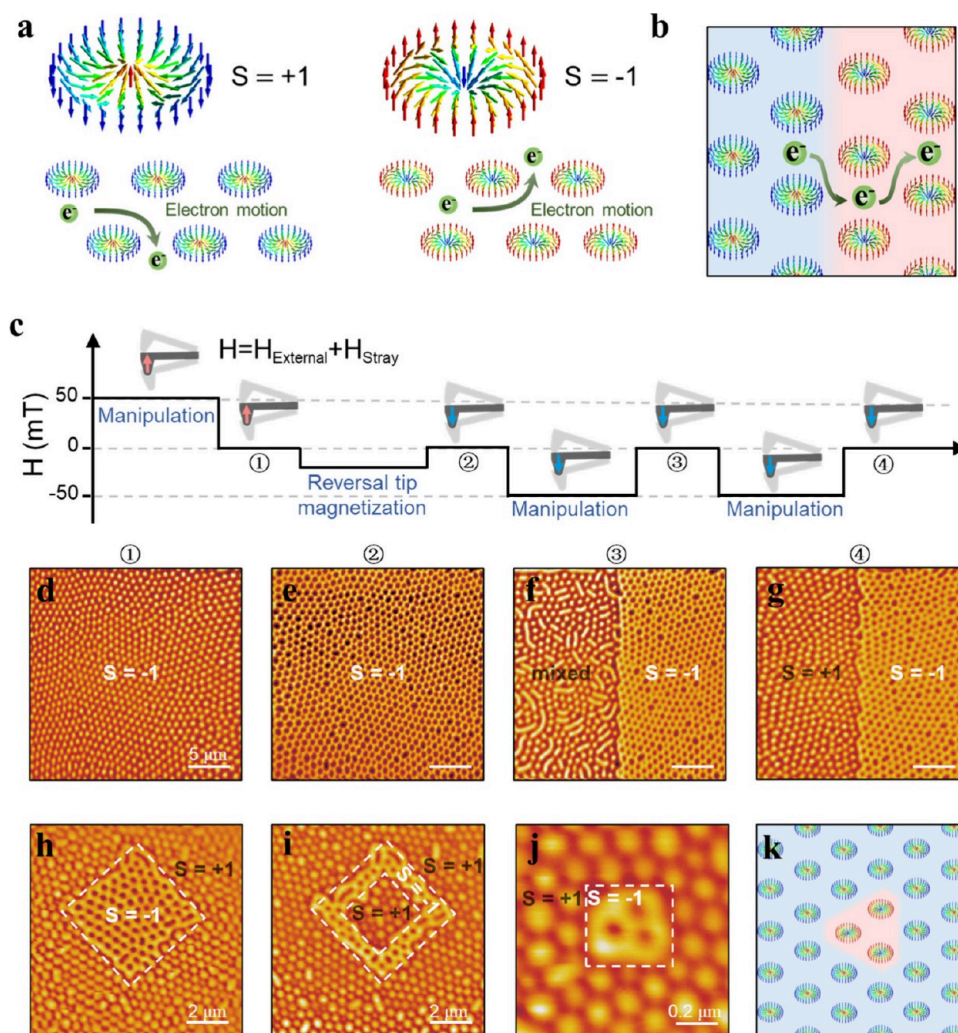
Figure 3. Topology-engineering of skyrmions on Fe_3GaTe_2 flake. (a) Schematic illustration of skyrmions with different topological charges ($S = \pm 1$). The lower insets show the motion of electrons influenced by skyrmions. (b) Schematic drawing of electron motion at the boundary of the skyrmion lattice with different topological charges. (c) Schematic drawing of the manipulation processed for realizing coexisting skyrmions with different topological charges. (d−g) Corresponding MFM images in (c). (h−j) MFM images after topology-engineering of skyrmions. The fine patterning of distinct topological skyrmions can be accomplished by using a magnetic tip. (k) Schematic drawing of different topological skyrmions in (j). Scale bar: (d−g) 5 μm; (h,i) 2 μm; (j) 0.2 μm.

of 0.03−0.08 T (Figure S3). The phase diagram of Fe_3GaTe_2 was constructed based on the experimental results, as shown in Figure 1j. In addition, we also examined the skyrmion lattices in Fe_3GaTe_2 flakes with varying thicknesses, and it is evident that the size of the skyrmions depends on the thickness (Figure S4). The exceptional storage density and high stability properties of magnetic skyrmions position them at the forefront of promising candidates for building next-generation information storage devices.[8,14,16,35,40−42] For a truly functional storage device, skyrmions must be able to be created and erased in a deterministic manner. In order to demonstrate the potential of Fe_3GaTe_2 as a next-generation storage device, we conducted further investigations into manipulating the topological spin texture in Fe_3GaTe_2 and successfully achieved the implementation of skyrmion painting and erasing.

The MFM setting illustrated in Figure 2a demonstrates the manipulation of the magnetic structures within a Fe_3GaTe_2 flake, where skyrmions are painted and erased by interacting with the stray field produced by the magnetic tip. The stray field of the magnetic tip may reach magnitudes in the

thousands of Gauss and exhibits rapid decay along the z-direction (Figure S5d).[10] Therefore, by adjusting the setpoint, we can effectively utilize MFM as either characterization or manipulation modes (Figure S5). In the manipulation mode, a uniform skyrmion lattice is successfully painted by applying an out-of-plane magnetic field (0.05T) along the z direction, consistent with the direction of the tip's stray field, the combination of the stray field of tip), as shown in Figure 2b. The density of the skyrmions can be varied with the number of manipulations. Performing the single manipulation results in a lower quantity of skyrmions, while seven manipulations essentially form a skyrmion lattice with a nearly hexagonal structure (Figure S6), which is consistent with previous studies, demonstrating the effectiveness of this method.[10,22,37] It is worth noting that written skyrmions remain stable below the saturation field and are unaffected by the external static magnetic field. The large-scale MFM image in Figure 2c displays a stable and homogeneous skyrmion lattice in the manipulation region, while the surrounding magnetic domains
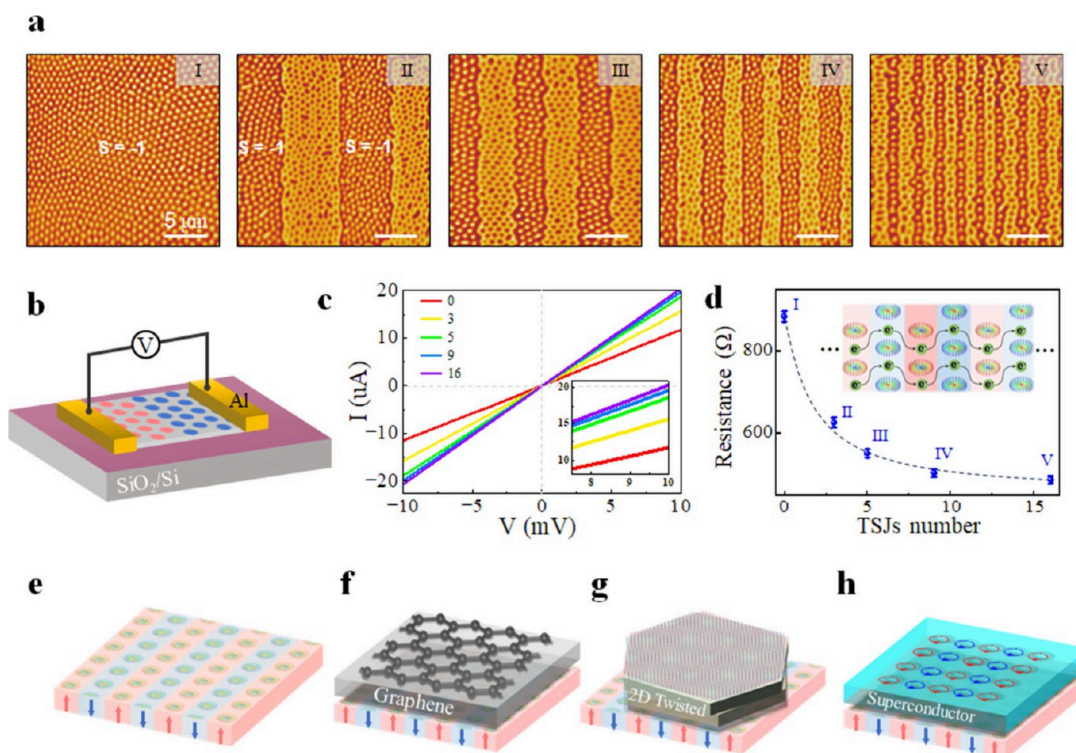
Figure 4. TSJ and resistance modulation action. (a) MFM images with different number of TSJs. (b) Schematic illustration of the resistance measuring device. (c,d) Current−voltage (I−V) curves (c) and resistance (d) of periodic skyrmion arrays in (a). The numerical values correspond to the number of TSJs present in different periodic skyrmion arrays. The inset in (d) shows the motion of electrons in TSJs. (e) Schematic diagram of TSJs with rows of single skyrmion. This particular topological magnetic structure exhibits spatially periodic magnetic fields and topological charges. (f−h) Schematic of stacking graphene (f), moiré pattern (g), and superconductors (h) on skyrmion arrays shown in (e). Scale bar: 5 μm.

remain primarily in a labyrinthine domain. The clear boundary indicates the high precision of our manipulation.

Skyrmion lattice generated through FC and painted through manipulation are further compared, as shown in Figure 2d−g. The distance between the manipulation-written skyrmions is slightly longer and exhibits higher homogeneity, forming an almost perfect hexagonal lattice when compared with the skyrmions created by simple FC. Furthermore, the MFM signals of each skyrmion generated in both methods exhibit minimal differences (Figure 2g), indicating their identical topological nature (vorticity). Afterward, we proceeded to manipulate the skyrmion lattice by erasing the skyrmions successfully at 0.17 T, as shown in Figures 2h,i. The numerical value within the central white dashed box indicates the quantity of manipulations. The skyrmions can be partially erased with a single manipulation, while complete disappearance of skyrmions occurs when the number of manipulations exceeds two. The subsequent MFM characterization with decreasing magnetic field reveals that in regions with a low density of skyrmions the descendance of magnetic field induces the formation of labyrinthine domains and destabilizes the surrounding skyrmions, as shown in Figures 2i−m.

So far, painting and erasing of the skyrmions in Fe_3GaTe_2 have been successfully achieved without relying on thermodynamics, thereby confirming the potential of Fe_3GaTe_2 as a next-generation storage device. The presence or absence of skyrmions can be utilized as a binary bit of 1 or 0, respectively. Note that the absence of skyrmions in certain regions may lead to formation of labyrinthine domains, which can negatively impact the performance of devices fabricated on Fe_3GaTe_2.

The highly manipulatable nature of the skyrmion lattice in Fe_3GaTe_2 prompts us to propose a novel approach for binary bit representation, i.e., the utilization of skyrmions with different topological charges. The following section presents our topology-engineering of skyrmions in Fe_3GaTe_2. We have successfully achieved the unprecedented coexistence of skyrmions with distinct topological charges and constructed a specific magnetic texture with unique electrical properties.

Skyrmions can indeed be defined by the topological charge S (or skyrmion number), which is a measure of the winding of the normalized local magnetization (m). In the two-dimensional limit, the topological number is[4,16,43]

$$S = \frac{1}{4\pi} \int m \cdot (\partial_x m \times \partial_y m) \mathrm{d}x\mathrm{d}y = \pm 1$$

The normalized magnetization can be mapped on a unit sphere, and in the case of skyrmions, it covers the entirety of the sphere (4π) and is thus quantized. In Fe_3GaTe_2, skyrmions exhibit a Néel-type configuration, characterized by radial-shaped spin textures and possessing 0- or 180-degrees helicity.[33] These topologically nontrivial chiral spin textures are characterized by topological charges $S = \pm 1$. The spin configurations with topological charges $S = \pm 1$ are illustrated in Figure 3a. Due to their nontrivial nature, skyrmions induce a topological Hall effect by acting as emergent electromagnetic fields, deflecting the motion of electrons. It is worth noting that the motion directions of electrons in $S = 1$ and $S = -1$ skyrmion lattices are opposite. Therefore, if electrons can traverse regions with opposing topological charges of skyrmions, their deflection of motion is effectively counter-
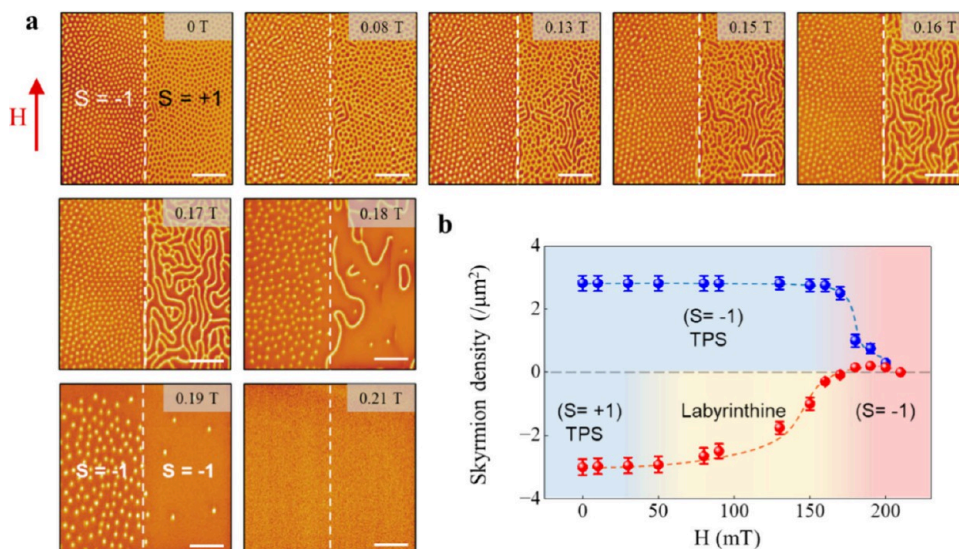
Figure 5. Topological properties of skyrmions with different topological charges. (a) MFM images of the TSJ with increasing magnetic fields. (b) The variation curve of skyrmion density with a magnetic field in the $S = +1$ and $S = -1$ regions. Scale bar: 4 μm.

acted,[16,44] thereby significantly enhancing the rate of longitudinal electron conductivity, as illustrated in Figure 3b.

The controllable generation of skyrmions with different topological charges can be achieved by reversing the magnetic tip's magnetization and the direction of the magnetic field, as shown in Figure 3c. The first step involves creation of a skyrmion lattice with $S = -1$ in Fe_3GaTe_2, with the magnetic field and the tip's magnetization aligned positively, as illustrated in Figure 3d. Subsequently, the reversal of the magnetic tip's magnetization causes the corresponding signal in the MFM image to invert as shown in Figure 3e. Following this, manipulation was performed in a specific region (left rectangle) of the skyrmion lattice with $S = -1$, where both the magnetic field and the tip's magnetization are negative. After multiple manipulations, it is evident that $S = 1$ skyrmions are generated in the manipulation region, as shown in Figure 3f. Following multiple manipulations, the manipulated region undergoes a complete transformation into an $S = 1$ skyrmion lattice, resulting in coexisting skyrmion lattices with distinct topological charges, as shown in Figure 3g. This coexisting phase is stable and exhibits stability at room temperature, even in the absence of an external magnetic field. We then named this special magnetic structure as a "topological skyrmion junction (TSJ)."

More detailed exploration of this method for painting skyrmion lattices with different topological charges reveals its high level of manipulability and precision. The manipulability of this painting method enables the realization of any desired complex pattern on Fe_3GaTe_2. Through a systematic experimental design, we successfully achieved intricate patterning on the skyrmion lattice of Fe_3GaTe_2, as shown in Figure 3h,i. The high precision of this painting method enables us to manipulate the magnetic texture more finely, even down to several individual skyrmions. Figure 3j,k shows the MFM image and corresponding schematic drawings after writing three skyrmions with opposite topological charges. It is worth mentioning that the switching between skyrmions with different topological charges is reversible and can be altered based on the selected area and the direction of the magnetic field. These results validate the extensive applicability of this

painting method, thereby offering novel insights and a platform for future development and investigation in storage devices based on skyrmions.

The proposed new method for manipulating skyrmions of different topological charges offers an opportunity to artificially construct TSJs, which can significantly enhance the electron transmission efficiency, as discussed previously. Following this, a series of periodic skyrmion arrays were constructed and their MFM images are depicted in Figure 4a. Notably, the minimum limit, that is, a single skyrmion periodic array, has been achieved. The periodic skyrmion arrays are distinguished by the number of TSJs present, which correspond to 0, 3, 5, 9, and 16 from left to right. To investigate the electrical properties of these periodic skyrmion arrays, resistance measurements were conducted on them using the experimental setup illustrated in Figure 4b. The measured current−voltage ($I-V$) curves in Figure 4c demonstrate a noticeable increase in the slope with the number of TSJs. By extracting the resistance of the various periodic skyrmion arrays based on these $I-V$ curves, the relationship between resistance and the number of TSJs is depicted in Figure 4d. The resistance decreases with the increase in the number of TSJs, since the deflection of electron motion is effectively counteracted when they pass through regions with skyrmions of opposite topological charges, in accordance with expectations. The above experimental results demonstrate that the implementation of TSJ can effectively enhance electron transmission rates, thereby resulting in reduced energy consumption and improved efficiency of electronic devices.

In addition to their unique electrical properties, TSJs can also be an excellent candidate for bottom substrates that modulate properties, of other samples through proximity effects. This particular topological magnetic structure not only facilitates the presence of periodic topological charges, but also enables generation of periodic magnetic fields, as shown in Figure 4e. Considering the challenge and importance of realizing spatial controllable periodic magnetic fields,[45] our findings could provide an opportunity to explore novel magnetic phenomena and their potential applications with the bottom substrate. For instance, if the electronic states and

band structures in two-dimensional materials such as graphene (Figure 4f) or moiré superlattices (Figure 4g) can be modulated, it may be possible to achieve intricate topological quantum states and pave the way for the development of quantum devices with exceptional properties.[46−51] Moreover, if the superconducting pairing channels in superconductors (Figure 4h) can be manipulated, unconventional or topologically nontrivial superconducting phases could be generated.[52−55]

Finally, we investigate the temperature stability and topological properties of TSJ in Fe_3GaTe_2. The MFM images obtained during the cooling process reveal that the TSJs exhibit variable temperature stability and can be effectively stabilized down to at least 200 K (Figure S7). Further magnetic-field-dependent MFM characterization reveals differences in the topological properties of skyrmions with different topological charges, as shown in Figure 5a. For skyrmion with $S = -1$, which is antiparallel to the magnetic field, remains stable below the saturation field and exists in a topologically protected state (TPS). Skyrmions gradually vanish near the saturation field as they are unable to maintain their spin texture, ultimately transitioning into the saturated state. In contrast, for the skyrmion with $S = 1$, which is parallel to the magnetic field, its spin texture is more susceptible to disruption caused by the magnetic field, and the TPS remains stable only up to 0.05 T. Subsequently, the skyrmions undergo fusion and expansion, resulting in compression of the background region into a labyrinthine domain. The labyrinthine domains undergo further fragmentation and contraction under the influence of the magnetic field, ultimately transforming into $S = -1$ skyrmions near the saturation field before eventually reaching the saturation state. The difference in the topological properties of the $S = 1$ and $S = -1$ skyrmion lattices can be intuitively visualized by examining the skyrmion density as a function of fields, as shown in Figure 5b.

In summary, our study highlights the potential of the 2D vdW ferromagnet Fe_3GaTe_2 as a platform for investigating and engineering topological textures with magnetic skyrmions. We found that painting and erasing of skyrmion lattices were successfully achieved by using a magnetic tip, eliminating the necessity of FC. We also successfully realized both $S = 1$ and $S = -1$ skyrmion lattices, as well as coexistence of both type of skyrmions. As an example, we fabricated a unique TSJ and found that it improves electron transmission rates with reduced device resistance. Finally, skyrmions with opposite topological charges exhibiting different field-dependence of skyrmiosn densities. Our results provide topological skyrmions as candidate platforms for development of future storage devices with binary representation and high-efficiency transport devices, and serving as a bottom substrate with spatially periodic magnetic fields, which opens a new route for investigating topological spintronics and new quantum states.

■ ASSOCIATED CONTENT

Ⓢ Supporting Information

The Supporting Information is available free of charge at https://pubs.acs.org/doi/10.1021/acs.nanolett.4c04031.

Materials and methods and supplementary figures showing details about labyrinthine domain, MFM settings, temperature dependence of skyrmions, etc. (PDF)

■ AUTHOR INFORMATION

Corresponding Authors

Xiaolei Wang − *School of Physics and Optoelectronic Engineering, Beijing University of Technology, Beijing 100124, China;* ⓞ orcid.org/0000-0002-6964-2453; Email: xiaoleiwang@bjut.edu.cn

Xueyun Wang − *School of Aerospace Engineering, Beijing Institute of Technology, Beijing 100081, China;* ⓞ orcid.org/0000-0001-5264-9539; Email: xueyun@bit.edu.cn

Haitao Yang − *Institute of Physics, Chinese Academy of Sciences, Beijing 100190, China;* Email: htyang@iphy.ac.cn

Zhihai Cheng − *Key Laboratory of Quantum State Construction and Manipulation (Ministry of Education) and Department of Physics and Beijing Key Laboratory of Optoelectronic Functional Materials & Micro-nano Devices, Renmin University of China, Beijing 100872, China;* ⓞ orcid.org/0000-0003-4938-4490; Email: zhihaicheng@ruc.edu.cn

Authors

Shuo Mi − *Key Laboratory of Quantum State Construction and Manipulation (Ministry of Education) and Department of Physics and Beijing Key Laboratory of Optoelectronic Functional Materials & Micro-nano Devices, Renmin University of China, Beijing 100872, China*

Jianfeng Guo − *Key Laboratory of Quantum State Construction and Manipulation (Ministry of Education) and Department of Physics and Beijing Key Laboratory of Optoelectronic Functional Materials & Micro-nano Devices, Renmin University of China, Beijing 100872, China; Institute of Physics, Chinese Academy of Sciences, Beijing 100190, China*

Guojing Hu − *Institute of Physics, Chinese Academy of Sciences, Beijing 100190, China*

Guangcheng Wang − *School of Physics and Optoelectronic Engineering, Beijing University of Technology, Beijing 100124, China*

Songyang Li − *Key Laboratory of Quantum State Construction and Manipulation (Ministry of Education) and Department of Physics and Beijing Key Laboratory of Optoelectronic Functional Materials & Micro-nano Devices, Renmin University of China, Beijing 100872, China*

Zizhao Gong − *Institute of Physics, Chinese Academy of Sciences, Beijing 100190, China*

Shuaizhao Jin − *School of Aerospace Engineering, Beijing Institute of Technology, Beijing 100081, China*

Rui Xu − *Key Laboratory of Quantum State Construction and Manipulation (Ministry of Education) and Department of Physics and Beijing Key Laboratory of Optoelectronic Functional Materials & Micro-nano Devices, Renmin University of China, Beijing 100872, China*

Fei Pang − *Key Laboratory of Quantum State Construction and Manipulation (Ministry of Education) and Department of Physics and Beijing Key Laboratory of Optoelectronic Functional Materials & Micro-nano Devices, Renmin University of China, Beijing 100872, China;* ⓞ orcid.org/0000-0002-8578-366X

Wei Ji − *Key Laboratory of Quantum State Construction and Manipulation (Ministry of Education) and Department of Physics and Beijing Key Laboratory of Optoelectronic Functional Materials & Micro-nano Devices, Renmin University of China, Beijing 100872, China;* ⓞ orcid.org/0000-0001-5249-6624

Weiqiang Yu − *Key Laboratory of Quantum State Construction and Manipulation (Ministry of Education) and Department of Physics and Beijing Key Laboratory of Optoelectronic Functional Materials & Micro-nano Devices, Renmin University of China, Beijing 100872, China*

Complete contact information is available at:
https://pubs.acs.org/10.1021/acs.nanolett.4c04031

Author Contributions

[+]These authors contributed equally to this work: Shuo Mi and Jianfeng Guo.

Notes

The authors declare no competing financial interest.

■ REFERENCES

(1) Rößler, U. K.; Bogdanov, A. N.; Pfleiderer, C. Spontaneous skyrmion ground states in magnetic metals. *Nature* **2006**, *442*, 797−801.

(2) Yu, X. Z.; Onose, Y.; Kanazawa, N.; Park, J. H.; Han, J. H.; Matsui, Y.; Nagaosa, N.; Tokura, Y. Real-space observation of a two-dimensional skyrmion crystal. *Nature* **2010**, *465*, 901−904.

(3) Nagaosa, N.; Tokura, Y. Topological properties and dynamics of magnetic skyrmions. *Nat. Nanotechnol.* **2013**, *8*, 899−911.

(4) Wang, L.; Feng, Q.; Kim, Y.; Kim, R.; Lee, K. H.; Pollard, S. D.; Shin, Y. J.; Zhou, H.; Peng, W.; Lee, D.; et al. Ferroelectrically tunable magnetic skyrmions in ultrathin oxide heterostructures. *Nat. Mater.* **2018**, *17*, 1087−1094.

(5) Fert, A.; Cros, V.; Sampaio, J. Skyrmions on the track. *Nat. Nanotechnol.* **2013**, *8*, 152−156.

(6) Kézsmárki, I.; Bordács, S.; Milde, P.; Neuber, E.; Eng, L. M.; White, J. S.; Rønnow, H. M.; Dewhurst, C. D.; Mochizuki, M.; Yanai, K.; et al. Néel-type skyrmion lattice with confined orientation in the polar magnetic semiconductor GaV$_4$S$_8$. *Nat. Mater.* **2015**, *14*, 1116−1122.

(7) Moreau-Luchaire, C.; Moutafis, C.; Reyren, N.; Sampaio, J.; Vaz, C. A. F.; Van Horne, N.; Bouzehouane, K.; Garcia, K.; Deranlot, C.; Warnicke, P.; et al. Additive interfacial chiral interaction in multilayers for stabilization of small individual skyrmions at room temperature. *Nat. Nanotechnol.* **2016**, *11*, 444−448.

(8) Schott, M.; Bernand-Mantel, A.; Ranno, L.; Pizzini, S.; Vogel, J.; Béa, H.; Baraduc, C.; Auffret, S.; Gaudin, G.; Givord, D. The Skyrmion Switch: Turning Magnetic Skyrmion Bubbles on and off with an Electric Field. *Nano Lett.* **2017**, *17*, 3006−3012.

(9) Maccariello, D.; Legrand, W.; Reyren, N.; Garcia, K.; Bouzehouane, K.; Collin, S.; Cros, V.; Fert, A. Electrical detection of single magnetic skyrmions in metallic multilayers at room temperature. *Nat. Nanotechnol.* **2018**, *13*, 233−237.

(10) Zhang, S.; Zhang, J.; Zhang, Q.; Barton, C.; Neu, V.; Zhao, Y.; Hou, Z.; Wen, Y.; Gong, C.; Kazakova, O.; et al. Direct writing of room temperature and zero field skyrmion lattices by a scanning local magnetic field. *Appl. Phys. Lett.* **2018**, *112*, No. 132405.

(11) Ognev, A. V.; Kolesnikov, A. G.; Kim, Y. J.; Cha, I. H.; Sadovnikov, A. V.; Nikitov, S. A.; Soldatov, I. V.; Talapatra, A.; Mohanty, J.; Mruczkiewicz, M.; et al. Magnetic Direct-Write Skyrmion Nanolithography. *ACS Nano* **2020**, *14*, 14960−14970.

(12) Jiang, W.; Zhang, X.; Yu, G.; Zhang, W.; Wang, X.; Benjamin Jungfleisch, M.; Pearson, J. E.; Cheng, X.; Heinonen, O.; Wang, K. L.; et al. Direct observation of the skyrmion Hall effect. *Nat. Phys.* **2017**, *13*, 162−169.

(13) Kimbell, G.; Kim, C.; Wu, W.; Cuoco, M.; Robinson, J. W. A. Challenges in identifying chiral spin textures via the topological Hall effect. *Commun. Mater.* **2022**, *3*, 19.

(14) Everschor-Sitte, K.; Sinova, J.; Abanov, A. Painting and erasing skyrmions. *Nat. Electron.* **2018**, *1*, 266−267.

(15) Raju, M.; Yagil, A.; Soumyanarayanan, A.; Tan, A. K. C.; Almoalem, A.; Ma, F.; Auslaender, O. M.; Panagopoulos, C. The evolution of skyrmions in Ir/Fe/Co/Pt multilayers and their topological Hall signature. *Nat. Commun.* **2019**, *10*, 696.

(16) Zhang, X.; Zhou, Y.; Mee Song, K.; Park, T.-E.; Xia, J.; Ezawa, M.; Liu, X.; Zhao, W.; Zhao, G.; Woo, S. Skyrmion-electronics: writing, deleting, reading and processing magnetic skyrmions toward spintronic applications. *J. Phys.: Condens. Matter* **2020**, *32*, No. 143001.

(17) Zhao, X.; Tang, J.; Pei, K.; Wang, W.; Lin, S.-Z.; Du, H.; Tian, M.; Che, R. Current-Induced Magnetic Skyrmions with Controllable Polarities in the Helical Phase. *Nano Lett.* **2022**, *22*, 8793−8800.

(18) Li, S.; Wang, X.; Rasing, T. Magnetic skyrmions: Basic properties and potential applications. *Interdisciplinary Mater.* **2023**, *2*, 260−289.

(19) Carteaux, V.; Brunet, D.; Ouvrard, G.; Andre, G. Crystallographic, magnetic and electronic structures of a new layered ferromagnetic compound Cr$_2$Ge$_2$Te$_6$. *J. Phys.: Condens. Matter* **1995**, *7*, 69.

(20) Wang, Z.; Gutiérrez-Lezama, I.; Ubrig, N.; Kroner, M.; Gibertini, M.; Taniguchi, T.; Watanabe, K.; Imamoğlu, A.; Giannini, E.; Morpurgo, A. F. Very large tunneling magnetoresistance in layered magnetic semiconductor CrI$_3$. *Nat. Commun.* **2018**, *9*, 2516.

(21) Deng, Y.; Yu, Y.; Song, Y.; Zhang, J.; Wang, N. Z.; Sun, Z.; Yi, Y.; Wu, Y. Z.; Wu, S.; Zhu, J.; et al. Gate-tunable room-temperature ferromagnetism in two-dimensional Fe$_3$GeTe$_2$. *Nature* **2018**, *563*, 94−99.

(22) Zhang, H.; Raftrey, D.; Chan, Y.-T.; Shao, Y.-T.; Chen, R.; Chen, X.; Huang, X.; Reichanadter, J. T.; Dong, K.; Susarla, S.; et al. Room-temperature skyrmion lattice in a layered magnet (Fe$_{0.5}$Co$_{0.5}$)$_5$GeTe$_2$. *Sci. Adv.* **2022**, *8*, 7103.

(23) Fei, Z.; Huang, B.; Malinowski, P.; Wang, W.; Song, T.; Sanchez, J.; Yao, W.; Xiao, D.; Zhu, X.; May, A. F.; et al. Two-dimensional itinerant ferromagnetism in atomically thin Fe$_3$GeTe$_2$. *Nat. Mater.* **2018**, *17*, 778−782.

(24) Kim, K.; Seo, J.; Lee, E.; Ko, K. T.; Kim, B. S.; Jang, B. G.; Ok, J. M.; Lee, J.; Jo, Y. J.; Kang, W.; et al. Large anomalous Hall current induced by topological nodal lines in a ferromagnetic van der Waals semimetal. *Nat. Mater.* **2018**, *17*, 794−799.

(25) Li, Q.; Yang, M.; Gong, C.; Chopdekar, R. V.; N'Diaye, A. T.; Turner, J.; Chen, G.; Scholl, A.; Shafer, P.; Arenholz, E.; et al. Patterning-Induced Ferromagnetism of Fe$_3$GeTe$_2$ van der Waals Materials beyond Room Temperature. *Nano Lett.* **2018**, *18*, 5974−5980.

(26) Pei, K.; Liu, S.; Yang, L.; Zhang, E.; Zhang, R.; Yang, C.; Ai, L.; Li, Z.; Xiu, F.; Che, R. Controllable Domain Walls in Two-Dimensional Ferromagnetic Material Fe$_3$GeTe$_2$ Based on the Spin-Transfer Torque Effect. *ACS Nano* **2021**, *15*, 19513−19521.

(27) Yang, C.; Huang, Y.; Pei, K.; Long, X.; Yang, L.; Luo, Y.; Lai, Y.; Zhang, J.; Cao, G.; Che, R. Current-Controllable and Reversible Multi-Resistance-State Based on Domain Wall Number Transition in 2D Ferromagnet Fe$_3$GeTe$_2$. *Adv. Mater.* **2024**, *36*, No. 2311831.

(28) Huang, M.; Wang, S.; Wang, Z.; Liu, P.; Xiang, J.; Feng, C.; Wang, X.; Zhang, Z.; Wen, Z.; Xu, H.; et al. Colossal Anomalous Hall Effect in Ferromagnetic van der Waals CrTe$_2$. *ACS Nano* **2021**, *15*, 9759−9763.

(29) Zhang, G.; Guo, F.; Wu, H.; Wen, X.; Yang, L.; Jin, W.; Zhang, W.; Chang, H. Above-room-temperature strong intrinsic ferromagnetism in 2D van der Waals Fe$_3$GaTe$_2$ with large perpendicular magnetic anisotropy. *Nat. Commun.* **2022**, *13*, 5067.

(30) Zhang, G.; Luo, Q.; Wen, X.; Wu, H.; Yang, L.; Jin, W.; Li, L.; Zhang, J.; Zhang, W.; Shu, H.; et al. Giant 2D Skyrmion Topological Hall Effect with Ultrawide Temperature Window and Low-Current Manipulation in 2D Room-Temperature Ferromagnetic Crystals. *Chin. Phys. Lett.* **2023**, *40*, No. 117501.

(31) Hu, G.; Guo, H.; Lv, S.; Li, L.; Wang, Y.; Han, Y.; Pan, L.; Xie, Y.; Yu, W.; Zhu, K.; et al. Room-Temperature Antisymmetric Magnetoresistance in van der Waals Ferromagnet Fe$_3$GaTe$_2$ Nanosheets. *Adv. Mater.* **2024**, *36*, No. 2403154.

(32) Li, Z.; Zhang, H.; Li, G.; Guo, J.; Wang, Q.; Deng, Y.; Hu, Y.; Hu, X.; Liu, C.; Qin, M.; et al. Room-temperature sub-100 nm Néel-type skyrmions in non-stoichiometric van der Waals ferromagnet Fe$_{3-x}$GaTe$_2$ with ultrafast laser writability. *Nat. Commun.* **2024**, *15*, 1017.

(33) Kajale, S. N.; Nguyen, T.; Chao, C. A.; Bono, D. C.; Boonkird, A.; Li, M.; Sarkar, D. Current-induced switching of a van der Waals ferromagnet at room temperature. *Nat. Commun.* **2024**, *15*, 1485.

(34) Chen, Z.; Yang, Y.; Ying, T.; Guo, J.-g. High-Tc Ferromagnetic Semiconductor in Thinned 3D Ising Ferromagnetic Metal Fe$_3$GaTe$_2$. *Nano Lett.* **2024**, *24*, 993−1000.

(35) Lv, X.; Lv, H.; Huang, Y.; Zhang, R.; Qin, G.; Dong, Y.; Liu, M.; Pei, K.; Cao, G.; Zhang, J.; et al. Distinct skyrmion phases at room temperature in two-dimensional ferromagnet Fe$_3$GaTe$_2$. *Nat. Commun.* **2024**, *15*, 3278.

(36) Jin, S.; Wang, Y.; Zheng, H.; Dong, S.; Han, K.; Wang, Z.; Wang, G.; Jiang, X.; Wang, X.; Hong, J.; et al. Thickness- and Field-Dependent Magnetic Domain Evolution in van der Waals Fe$_3$GaTe$_2$. *Nano Lett.* **2024**, *24*, 5467−5473.

(37) Jin, S.; Wang, Z.; Dong, S.; Wang, Y.; Han, K.; Wang, G.; Deng, Z.; Jiang, X.; Zhang, Y.; Huang, H.; et al. Local manipulation of skyrmion lattice in Fe$_3$GaTe$_2$ at room temperature. *J. Materiomics* **2025**, *11*, No. 100865.

(38) Hou, X.; Wang, H.; Zhang, B.; Xu, C.; Sun, L.; Li, Z.; Wang, X.; Qu, K.; Wei, Y.; Guo, Y. Room-temperature skyrmions in the van der Waals ferromagnet Fe$_3$GaTe$_2$. *Appl. Phys. Lett.* **2024**, *124*, No. 142404.

(39) Zhang, C.; Jiang, Z.; Jiang, J.; He, W.; Zhang, J.; Hu, F.; Zhao, S.; Yang, D.; Liu, Y.; Peng, Y.; et al. Above-room-temperature chiral skyrmion lattice and Dzyaloshinskii−Moriya interaction in a van der Waals ferromagnet Fe$_{3-x}$GaTe$_2$. *Nat. Commun.* **2024**, *15*, 4472.

(40) Jonietz, F.; Mühlbauer, S.; Pfleiderer, C.; Neubauer, A.; Münzer, W.; Bauer, A.; Adams, T.; Georgii, R.; Böni, P.; Duine, R. A.; et al. Spin Transfer Torques in MnSi at Ultralow Current Densities. *Science* **2010**, *330*, 1648−1651.

(41) Siegl, P.; Stier, M.; Schäffer, A. F.; Vedmedenko, E. Y.; Posske, T.; Wiesendanger, R.; Thorwart, M. Creating arbitrary sequences of mobile magnetic skyrmions and antiskyrmions. *Phys. Rev. B* **2022**, *106*, No. 014421.

(42) Song, D.; Wang, W.; Zhang, S.; Liu, Y.; Wang, N.; Zheng, F.; Tian, M.; Dunin-Borkowski, R. E.; Zang, J.; Du, H. Steady motion of 80-nm-size skyrmions in a 100-nm-wide track. *Nat. Commun.* **2024**, *15*, 5614.

(43) Zhang, Y.; Tang, J.; Wu, Y.; Shi, M.; Xu, X.; Wang, S.; Tian, M.; Du, H. Stable skyrmion bundles at room temperature and zero magnetic field in a chiral magnet. *Nat. Commun.* **2024**, *15*, 3391.

(44) Jiang, W.; Chen, G.; Liu, K.; Zang, J.; te Velthuis, S. G. E.; Hoffmann, A. Skyrmions in magnetic multilayers. *Phys. Rep.* **2017**, *704*, 1−49.

(45) Shi, H.; Zhan, Z.; Qi, Z.; Huang, K.; Veen, E. v.; Silva-Guillén, J. Á.; Zhang, R.; Li, P.; Xie, K.; Ji, H.; et al. Large-area, periodic, and tunable intrinsic pseudo-magnetic fields in low-angle twisted bilayer graphene. *Nat. Commun.* **2020**, *11*, 371.

(46) Chamanara, N.; Caloz, C. Multiscale and multiphysics graphene sheet - magnetic nanowire gyrotropic metamaterial. In *2014 IEEE Antennas and Propagation Society International Symposium (APSURSI)*, Memphis, July 6−11, 2014; IEEE, 2014; pp 888−889.

(47) Zhang, S.; Jin, L.; Lu, Y.; Zhang, L.; Yang, J.; Zhao, Q.; Sun, D.; Thompson, J. J. P.; Yuan, B.; Ma, K.; et al. Moiré superlattices in twisted two-dimensional halide perovskites. *Nat. Mater.* **2024**, *23*, 1222−1229.

(48) Cao, Y.; Fatemi, V.; Fang, S.; Watanabe, K.; Taniguchi, T.; Kaxiras, E.; Jarillo-Herrero, P. Unconventional superconductivity in magic-angle graphene superlattices. *Nature* **2018**, *556*, 43−50.

(49) Wang, T.; Yuan, N. F. Q.; Fu, L. Moiré Surface States and Enhanced Superconductivity in Topological Insulators. *Phys. Rev. X* **2021**, *11*, No. 021024.

(50) Liu, Y.; Rodrigues, J. N. B.; Luo, Y. Z.; Li, L.; Carvalho, A.; Yang, M.; Laksono, E.; Lu, J.; Bao, Y.; Xu, H.; et al. Tailoring sample-wide pseudo-magnetic fields on a graphene−black phosphorus heterostructure. *Nat. Nanotechnol.* **2018**, *13*, 828−834.

(51) Kang, D.-H.; Sun, H.; Luo, M.; Lu, K.; Chen, M.; Kim, Y.; Jung, Y.; Gao, X.; Parluhutan, S. J.; Ge, J.; et al. Pseudo-magnetic field-induced slow carrier dynamics in periodically strained graphene. *Nat. Commun.* **2021**, *12*, 5087.

(52) Jeon, G. S.; Jain, J. K.; Liu, C. X. Topological superconductivity in Landau levels. *Phys. Rev. B* **2019**, *99*, No. 094509.

(53) Dobrovolskiy, O. V.; Sachser, R.; Brächer, T.; Böttcher, T.; Kruglyak, V. V.; Vovk, R. V.; Shklovskij, V. A.; Huth, M.; Hillebrands, B.; Chumak, A. V. Magnon-fluxon interaction in a ferromagnet/superconductor heterostructure. *Nat. Phys.* **2019**, *15*, 477−482.

(54) Zhang, P.; Yaji, K.; Hashimoto, T.; Ota, Y.; Kondo, T.; Okazaki, K.; Wang, Z.; Wen, J.; Gu, G. D.; Ding, H.; et al. Observation of topological superconductivity on the surface of an iron-based superconductor. *Science* **2018**, *360*, 182−186.

(55) Nikolaenko, A.; Pientka, F. Topological superconductivity in proximity to type-II superconductors. *Phys. Rev. B* **2021**, *103*, No. 134503.